

Signatures of the chiral two-pion exchange electromagnetic currents in the ${}^2\text{H}$ and ${}^3\text{He}$ photodisintegration reactions

D. Rozpędzik,¹ J. Golak,¹ S. Kölling,^{2,3} E. Epelbaum,⁴ R. Skibiński,¹ H. Witała,¹ and H. Krebs⁴

¹*M. Smoluchowski Institute of Physics, Jagiellonian University, PL-30059 Kraków, Poland*

²*Forschungszentrum Jülich, Institut für Kernphysik (IKP-3) and Jülich Center for Hadron Physics, D-52425 Jülich, Germany*

³*Helmholtz-Institut für Strahlen- und Kernphysik (Theorie) and Bethe Center for Theoretical Physics, Universität Bonn, D-53115 Bonn, Germany*

⁴*Institut für Theoretische Physik II, Ruhr-Universität Bochum, D-44780 Bochum, Germany*

(Dated: October 31, 2018)

The recently derived long-range two-pion exchange (TPE) contributions to the nuclear current operator which appear at next-to-leading order (NLO) of the chiral expansion are used to describe electromagnetic processes. We study their role in the photodisintegration of ${}^2\text{H}$ and ${}^3\text{He}$ and compare our predictions with experimental data. The bound and scattering states are calculated using five different parametrizations of the chiral next-to-next-to-leading order (N^2LO) nucleon-nucleon (NN) potential which allows us to estimate the theoretical uncertainty at a given order in the chiral expansion. For some observables the results are very close to the predictions based on the AV18 NN potential and the current operator (partly) consistent with this force. In the most cases, the addition of long-range TPE currents improved the description of the experimental data.

PACS numbers: 25.20-x, 21.45.-v, 24.70.+s

Keywords: ChEFT, electromagnetic reactions, meson exchange currents

I. INTRODUCTION

Chiral Effective Field Theory (ChEFT) provides a systematic and model-independent framework to analyze hadron structure and dynamics in harmony with the spontaneously broken approximate chiral symmetry of QCD. This approach is a powerful tool for the derivation of the nuclear forces. Exchange vector and axial currents in nuclei have also been studied in the framework of ChEFT. Since the pioneering work of Park et al. [1], heavy-baryon chiral perturbation theory has been applied to derive exchange axial and vector currents for small values of the photon momentum. These calculations have been carried out in time-ordered perturbation theory. The resulting exchange vector currents have been, in particular, applied to analyze radiative neutron-proton capture within a hybrid approach [2].

ChEFT has also been used to study the electromagnetic properties of the deuteron [3, 4] and ${}^3\text{He}$ [5, 6]. One of the fundamental processes observed for the deuteron is the photodisintegration reaction. It has been a subject of intense experimental and theoretical research for several decades (see Refs [7, 8]). Also photodisintegration of ${}^3\text{He}$ has been studied experimentally and theoretically for a long time [9–11]. Photodisintegration observables provide a good tool for studying the contributions from meson exchange currents (MEC) to the nuclear current operator. This is because the charge density operator, which often dominates low-energy electrodisintegration and is mostly given by the single nucleon current, does not play any role in this reaction. An ongoing interest in low-energy photodisintegration reactions, especially in view of planned experiments, provides a strong motivation to apply the framework of chiral effective field theory. This approach relies on the approximate spontaneously broken chiral symmetry of QCD. It allows for a systematic derivation of the nuclear Hamiltonian and the corresponding electromagnetic current operator from the underlying effective Lagrangian for pions and nucleons via the chiral expansion, i.e. a simultaneous expansion in soft momenta of external particles and about the chiral limit. For more details on the application of ChEFT to nuclear forces and currents the reader is referred to recent review articles [12, 13] and references therein.

In the two- and three-nucleon systems, the leading contributions to the exchange current originate from one-pion exchange which are well known. The 2N current operator at the leading loop order in the chiral expansion has been worked out by Pastore et al. [14, 15] based on time-ordered perturbation theory. Independently, the two-pion exchange 2N current operator has been derived in Ref. [16] using the method of unitary transformation. The resulting current operator is consistent with the corresponding chiral two-nucleon potential [12] obtained within the same scheme. In the present work, for the first time we explore the effects of the leading two-pion exchange 2N operator [16] in the photodisintegration reactions of ${}^2\text{H}$ and ${}^3\text{He}$. We, however, emphasize that the presented calculations are not yet complete. In particular, the corresponding expressions for the one-pion exchange at NLO and short-range contributions to the current operator within the method of unitary transformation are not yet available. Our main goal in the present work is to explore the sensitivity of various observables in the deuteron and ${}^3\text{He}$ photodisintegration to the two-pion exchange current rather than to provide a complete description of these reactions within the ChEFT framework.

Our manuscript is organized as follows. In section II the formalism which we use to describe selected 2N electromagnetic reactions is presented. The results for the photodisintegration of the ^2H are discussed and compared with the experimental data in section III. The extension to the 3N system is briefly described in section IV and the results obtained for photodisintegration of ^3He are presented in Section V. Finally, section VI contains the summary and conclusions.

II. FORMALISM

The general form of the nuclear matrix element for electromagnetic disintegration reactions in the 2N system is represented by

$$N^\mu \equiv \langle \Psi_{\text{scatt}}^{2N} | J^\mu(\vec{Q}) | \Psi_{\text{bound}}^{2N} \rangle, \quad (2.1)$$

where the proton-neutron scattering state $|\Psi_{\text{scatt}}^{2N}\rangle$ and the deuteron bound state $|\Psi_{\text{bound}}^{2N}\rangle$ are obtained using NN potential. The current operator $J^\mu(\vec{Q})$ acts between the internal initial and final 2N states. We employ the solution of the Lippmann-Schwinger equation, $t = V_{2N} + tG_0V_{2N}$, in order to express N^μ as

$$N^\mu = \langle \vec{p}_0 | (1 + tG_0) J^\mu(\vec{Q}) | \Psi_{\text{bound}}^{2N} \rangle, \quad (2.2)$$

where G_0 is the free 2N propagator, t is the NN t-matrix and $|\vec{p}_0\rangle$ is the eigenstate of the relative proton-neutron momentum. Since all observables can be computed from N^μ , the description of the electromagnetic reactions requires the knowledge of the consistent potential and electromagnetic current. The NN potential based on ChEFT is currently available up to next-to-next-to-next-to-leading order in the chiral expansion [12, 13]. As already pointed out, in this paper we focus on the long-range TPE contributions to the current operator, which appear at NLO. However, in order to avoid the theoretical error from using the less accurate NLO NN potential, all calculations are made using the N²LO potential. At this order, the NN potential V_{2N} is built from the one-pion exchange (OPE), $V_{1\pi}$, and two-pion exchange (TPE), $V_{2\pi}$, contributions as well as various contact interactions (cont) [12]

$$V_{2N} = V_{1\pi} + V_{2\pi} + V_{\text{cont}}. \quad (2.3)$$

The effective current operator J^μ for the 2N system is a sum of the single-nucleon operators $J^\mu(i)$, $i = 1, 2$ and two-nucleon operators of different type ($J^\mu(1, 2)$)

$$J^\mu = J^\mu(1) + J^\mu(2) + J^\mu(1, 2), \quad (2.4)$$

where

$$J^\mu(1, 2) = J_{1\pi}^\mu(1, 2) + J_{2\pi}^\mu(1, 2) + J_{\text{cont}}^\mu(1, 2). \quad (2.5)$$

The expressions for the single-nucleon and the leading OPE currents $J_{1\pi}^\mu(1, 2)$ are well established, see e.g. [17]. The results for the leading two-pion exchange contributions used in the present work are available in Refs. [14, 16]. We emphasize that the resulting two-pion exchange current is parameter-free. The expressions for the OPE and contact currents at the leading loop level have been recently worked out within time-ordered perturbation theory [15]. Work on the derivation of these contributions using the method of unitary transformation is still in progress.

The 2N four-current operator $J^\mu(1, 2) \equiv (J^0(1, 2), \vec{J}(1, 2))$ can be decomposed according to its isospin and spin-momentum structure and quite generally written in the form [16, 18]

$$J^0(1, 2) = \sum_{\eta=1}^5 \sum_{\beta=1}^8 f_\eta^{\beta S}(\vec{q}_1, \vec{q}_2) T_\eta O_\beta^S, \quad (2.6)$$

$$\vec{J}(1, 2) = \sum_{\eta=1}^5 \sum_{\beta=1}^{24} f_\eta^\beta(\vec{q}_1, \vec{q}_2) T_\eta \vec{O}_\beta, \quad (2.7)$$

where $\vec{q}_i \equiv \vec{p}'_i - \vec{p}_i$ is the momentum transferred to nucleon i , T_η is the 2N isospin operator, O_β^S and \vec{O}_β are the (momentum dependent) spin operators in the 2N space, $f_\eta^{\beta S}$ and f_η^β are scalar functions. The explicit form of the scalar functions and the operator basis for O_β^S and \vec{O}_β can be found in Ref. [16].

In this paper, we concentrate on a treatment of the long-range TPE contributions to the 2N current operator derived in Ref. [16]. The expressions for the functions $f_\eta^{\beta S}(\vec{q}_1, \vec{q}_2)$ and $f_\eta^\beta(\vec{q}_1, \vec{q}_2)$ entering the TPE current and charge density operators in Eqs. (2.6), (2.7) are rather complicated and contain the standard loop functions and the three-point

functions in a form suitable for numerical calculations [16]. Due to their isospin structure, not all combinations of (2.6) and (2.7) contribute to photodisintegration of the deuteron. The non-vanishing contributions emerge from

$$\vec{J}_{2\pi}(1, 2) = \sum_{\beta=3}^{10} f_2^\beta(\vec{q}_1, \vec{q}_2) (\vec{\tau}_1 - \vec{\tau}_2)_3 \vec{O}_\beta + f_3^2(\vec{q}_1, \vec{q}_2) (\vec{\tau}_1 \times \vec{\tau}_2)_3 \vec{O}_2, \quad (2.8)$$

where $(\dots)_3$ denotes the third cartesian component of the vector. We work in momentum space and apply the standard partial wave decomposition of the 2N potential, see e.g. Ref. [19] for more details. Our calculations are performed using a complete set of 2N states

$$|p\alpha\rangle \equiv |p(ls)jm_j\rangle|tm_t\rangle \quad (2.9)$$

where p is the magnitude of the relative momentum, l , s , j and m_j are the orbital angular momentum, spin, total angular momentum and its projection on the quantisation axis \hat{z} , respectively. The isospin quantum numbers of the two-nucleon system are denoted by t and m_t .

The TPE current operator needs to be expressed in the same partial wave basis. To this end, we first prepare all spin and isospin matrix elements using *Mathematica*© and then calculate the resulting four-fold angular integrals

$$\begin{aligned} \langle p'\alpha'|\vec{J}_{2\pi}(1, 2)|p\alpha\rangle &= \langle p'(l's')j'm_{j'}; t'm_{t'}|\vec{J}_{\eta\beta}|p(ls)jm_j; tm_t\rangle \quad (2.10) \\ &= \int d\hat{p}' d\hat{p} \sum_{m_l, m_l'} C(l's'j'; m_{l'}, m_{j'} - m_{l'}, m_{j'}) Y_{l'm_{l'}}^*(\hat{p}') C(ls j; m_l, m_j - m_l, m_j) Y_{l m_l}(\hat{p}) \\ &\times f_\eta^\beta(\vec{q}_1, \vec{q}_2) \langle t'm_{t'}|T_\eta|tm_t\rangle \langle s'm_{j'} - m_{l'}|\vec{O}_\beta|sm_j - m_l\rangle, \end{aligned}$$

numerically. Here, $C(ls j; m_l, m_j - m_l, m_j)$ denote the Clebsch-Gordon coefficient and $Y_{lm_l}(\hat{p})$ are the spherical harmonics. Such an approach has been described in Ref. [20]. In order to calculate the four-fold integrals in Eq. (2.10) for the whole grids of p and p' points and all non-vanishing (α, α', m_j) combinations we used the parallel supercomputer IBM Blue Gene/P of the Jülich Supercomputing Centre (JSC).

III. RESULTS FOR PHOTODISINTEGRATION OF THE DEUTERON

We now discuss the results for the deuteron photodisintegration process for the unpolarized cross section and selected polarization observables. The results for the differential cross section, the photon analyzing power and outgoing proton polarization at the photon laboratory energies of $E_\gamma = 10, 30$ and 60 MeV are shown in Fig. 1. The bands reflect the uncertainty due to the variation of the two cut-off parameters Λ and $\tilde{\Lambda}$ that appear in the chiral potential. While the first cut-off parameter Λ appears in the regulator function for the Lippmann-Schwinger equation, the second parameter $\tilde{\Lambda}$ enters the spectral function regularization (SFR) and denotes the ultraviolet cut-off value in the mass spectrum of the two-pion exchange potential. Following Ref. [12], the cut-off values are varied between 450 and 600 MeV for Λ and between 500 and 700 MeV for $\tilde{\Lambda}$. It is important to emphasize that the resulting bands probably overestimate the theoretical uncertainty that can be expected in a complete calculation at this order in the chiral expansion. This is because we have not yet included the corresponding short-range contributions to the nuclear current, which are expected to absorb the large part of the cut-off dependence. Thus, the interpretation of the band width in the obtained results in terms of the theoretical uncertainty should be taken with care. Different bands shown in Fig. 1 describe the contributions from the different parts of the 2N current: single-nucleon current (light band), one-pion exchange contribution (hatched band) and the long-range TPE contributions (dark band). As a reference, we also show the results based on the phenomenological AV18 potential [21] and the corresponding current model [22, 23]. Notice that the results obtained solely from the single nucleon currents and by adding the OPE contributions do not describe the data well and differ significantly from the reference AV18 predictions. An explicit inclusion of the TPE contributions yields an improved description of the experimental data which turns out to be in agreement with the AV18 predictions. The OPE predictions give the cross section and photon analyzing power values lower than the AV18 results. The bands including TPE currents are broad, however, for $E_\gamma = 30$ and 60 MeV they give reasonable description of the experimental data. In the case of photon analyzing powers, the best agreement between all models is obtained at lowest energy. For energies $E_\gamma = 30$ and 60 MeV, calculations including the TPE currents yield even better agreement with experimental data than the AV18 results. It remains to be seen whether this conclusion will still hold after including the short-range and the subleading OPE currents. It is further important to emphasize that the single nucleon current alone is insufficient to describe the data for this observable. Thus, it is necessary to include higher order electromagnetic currents. In the case of the outgoing proton polarization, we observe a smaller sensitivity to the TPE currents and a good agreement between traditional framework (AV18) and chiral results at all energies

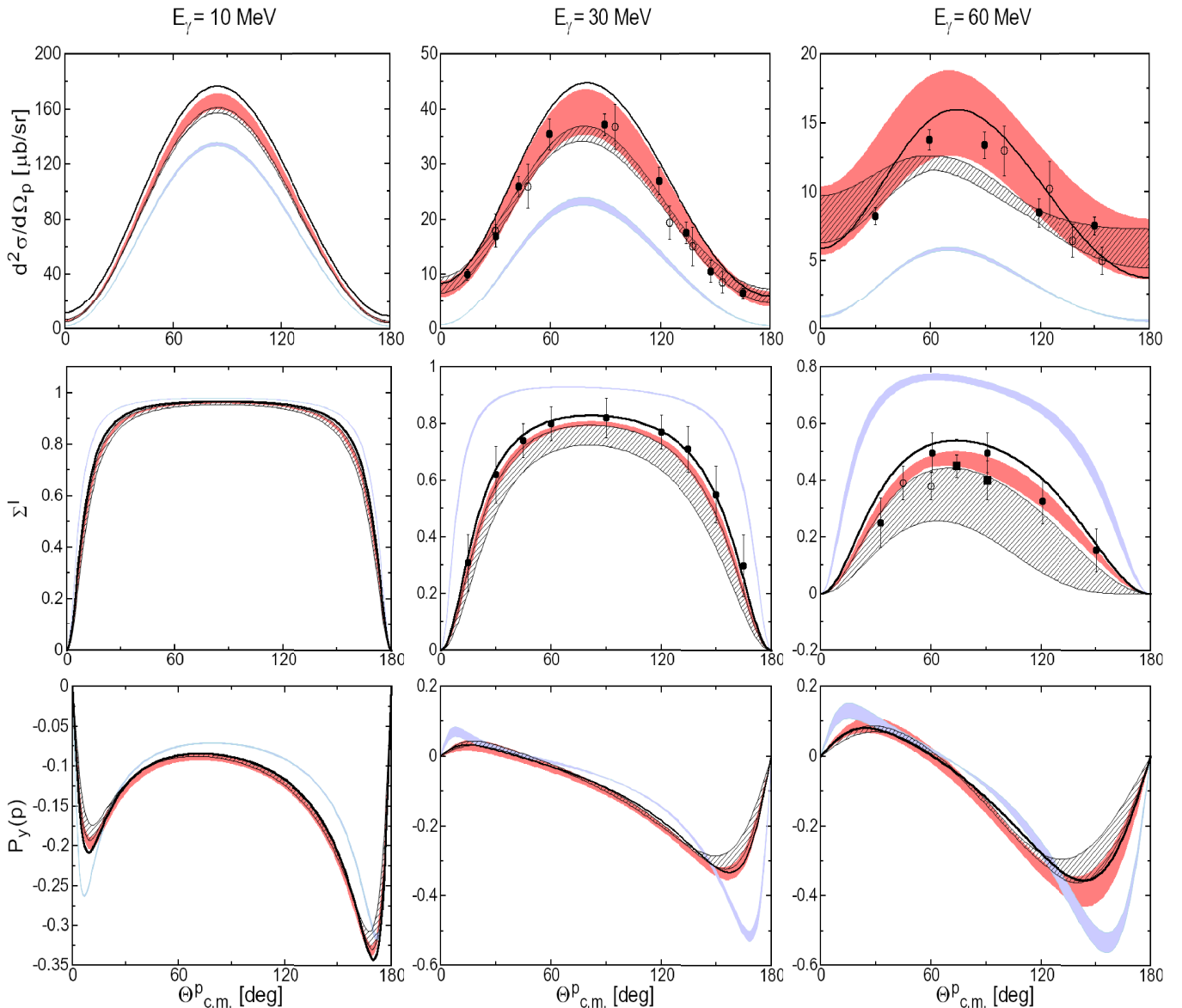


FIG. 1: (color online) The results for the unpolarized cross section, the photon analyzing power and outgoing proton polarization in the deuteron photodisintegration process at the photon laboratory energies of $E_\gamma = 10, 30, 60$ MeV, displayed as functions of the proton emission angle. The solid black line refers to the standard calculation based on the AV18 potential, the light (blue) band covers results obtained with the single-nucleon current only, the hatched band represents the predictions based on the single-nucleon and OPE parts and the dark (pink) band includes, in addition, the contributions of the TPE current. The experimental data are from Ying et al. [25].

considered. The larger sensitivity to the details of the exchange currents is only observed at forward and backward outgoing proton angles.

We have also calculated the deuteron tensor analyzing powers as a function of the proton emission angle for two E_γ - energy bins. Here, we focus on a comparison of our calculations with recent experimental tensor analyzing powers T_{2q} for low energies from [24] and do not show the results for vector analyzing power iT_{11} as there exist no experimental data for this observable. In order to be able to compare the theoretical calculations with the data from [24], our predictions for the exclusive observables have been integrated over the relevant intervals of the initial photon energy and angular regions. In Fig. 2 the results for the angular distribution at the bin energies of $E_\gamma = 25 - 45$ MeV and $E_\gamma = 45 - 70$ MeV together with experimental data are presented. For all deuteron tensor analyzing powers one observes a rather good agreement between the AV18 potential prediction, chiral results and experimental data. The effects of the TPE contributions turn out to be very small. Also, no broadening of the bands with increasing photon energy is observed. All this suggests that the deuteron tensor analyzing powers are driven by the long-range parts of the current and are not sensitive to the short-range contributions. We further emphasize some disagreement with the

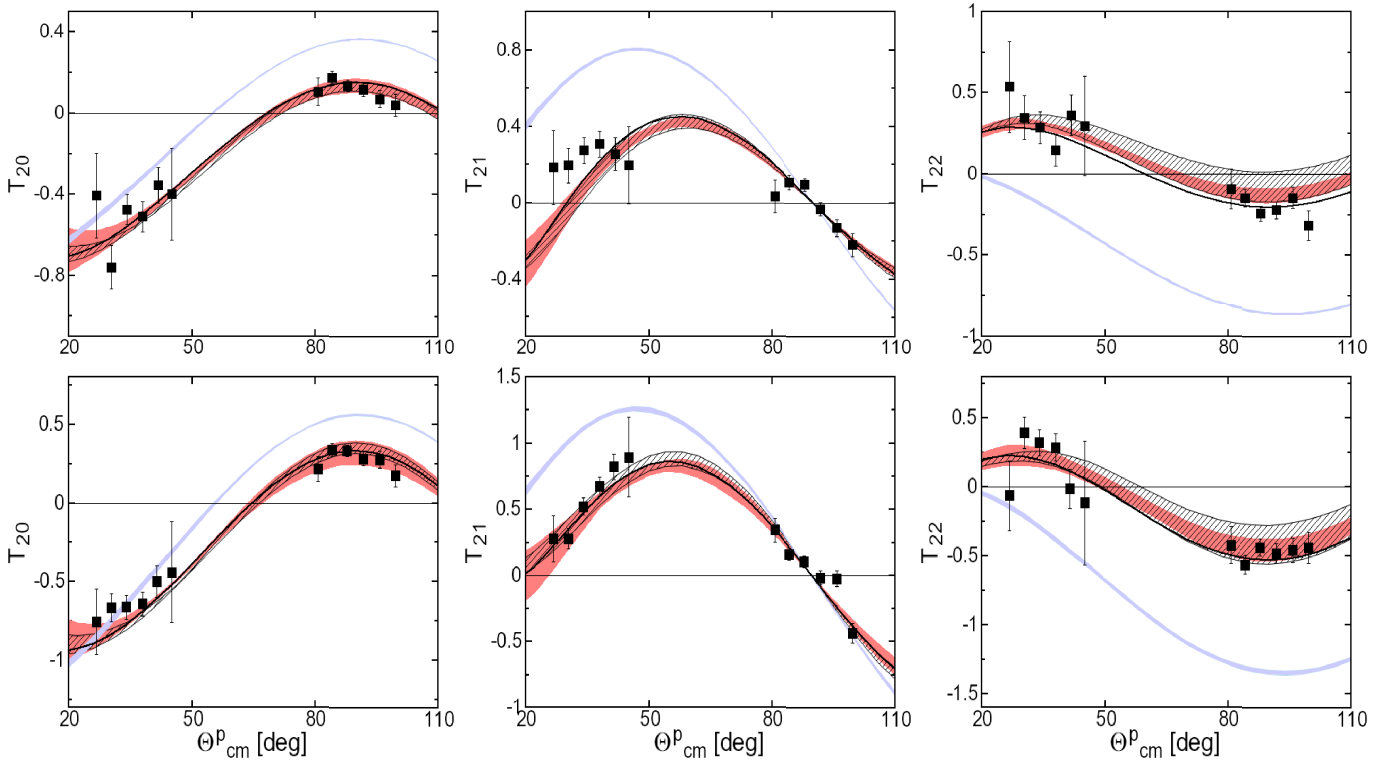


FIG. 2: (color online) Deuteron tensor analyzing powers vs. proton emission angle for two E_γ -energy bins. The upper row shows results for bin energy $E_\gamma = 25\text{-}45$ MeV. The lower row shows results for bin energy $E_\gamma = 45\text{-}70$ MeV. The bands and lines have the same meaning as in Fig. 1. The experimental data are from Rachek et al. [24].

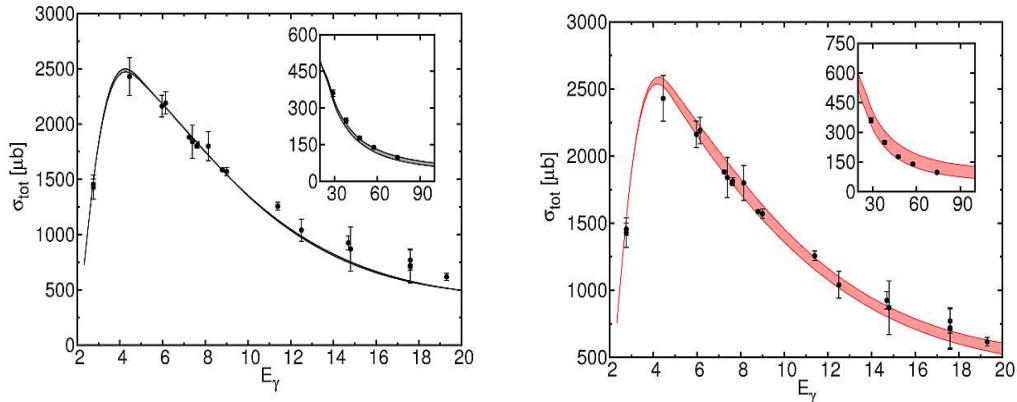


FIG. 3: (color online) Total cross section for photodisintegration of the deuteron as a function of photon energy beam. In the left panel results for the single nucleon current and OPE contribution are shown. In the right panel, the results obtained with an additional TPE currents are given. The experimental data are the same as in Ref. [7].

data for T_{21} at forward angles. In the future, it would be interesting to see whether these conclusions are affected by the inclusion of the subleading OPE terms in the current operator.

Finally, we have also calculated the total cross section. This observable was extensively studied in many publications using various theoretical approaches, see e.g. [7]. In Fig. 3, the total cross section for $E_\gamma \approx 2\text{-}80$ MeV is presented. The experimental data are taken from Refs. [7, 8]. In the left panel, we see the results for the single nucleon and OPE current. For this particular case the width of the prediction band is negligible. The theoretical predictions agree rather well with the experimental data. The right panel in this figure shows that the effects of the TPE currents are clearly visible, especially at higher photon energies. We also notice that the band width increases significantly once the TPE contributions are included.

To conclude, we observe that for all considered observables the 2N current operator plays an important role and

a restriction to the single nucleon current operator leads to a strong disagreement with the data. The inclusion of the leading OPE current is absolutely necessary to achieve a decent description of the experimental data. The effects of the TPE current are clearly visible in the differential cross section and some polarization observables such as Σ^1 and P_y . One also observes a rather good agreement between the results based on chiral EFT and the AV18 potential combined with the corresponding current operators.

IV. TWO-PION EXCHANGE CURRENTS IN THE 3N SYSTEM

For 3N reactions, we use the framework and its numerical implementation described in detail in [11]. In this work, we will only briefly introduce the key points focusing mainly on the current operator in the 3N system. The starting point is exactly the same as for the 2N reaction. We consider the general matrix element of the current operator between the 3N bound state, $|\Psi_{\text{bound}}^{3N}\rangle$, and scattering state $|\Psi_{\text{scatt}}^{3N}\rangle$ for the 3N system

$$N^\mu \equiv \langle \Psi_{\text{scatt}}^{3N} | J^\mu(\vec{Q}) | \Psi_{\text{bound}}^{3N} \rangle. \quad (4.1)$$

The 3N bound state $|\Psi_{\text{bound}}^{3N}\rangle$ is obtained in the standard way from the appropriate Faddeev equation [26]. The current operator $J^\mu(\vec{Q})$ acts effectively between the internal initial and final 3N states. These internal states are conventionally expressed in the momentum space in terms of two Jacobi momenta, \vec{p} and \vec{q} [19]. The momentum \vec{p} describes a relative motion within a 2N subsystem (here we choose the subsystem consisting of nucleons 2 and 3). The momentum \vec{q} describes the motion of the spectator nucleon (here nucleon 1) with respect to that 2N subsystem

$$\vec{p} = \frac{1}{2}(\vec{p}_2 - \vec{p}_3), \quad \vec{q} = \frac{2}{3}\left(\vec{p}_1 - \frac{1}{2}(\vec{p}_2 + \vec{p}_3)\right). \quad (4.2)$$

We consider two types of 3N scattering states. In the first case two nucleons bound in the deuteron emerge with the accompanying third nucleon and the asymptotic motion of this unbound nucleon is described by the Jacobi momentum \vec{q}_0 . In the second case, we have three free nucleons in the final state and their asymptotic relative motions are represented by \vec{p} and \vec{q} .

In order to calculate the crucial matrix elements N^μ given in (4.1), it is not necessary to solve the corresponding Faddeev equations directly for the 3N scattering states [11]. Instead, we solve a Faddeev-type equation for an auxiliary state $|U\rangle$. In our calculations, we do not include the effects of 3N forces. Thus, the equation for $|U\rangle$ takes a simpler form

$$|U\rangle = tG_0(1+P)J^\mu(\vec{Q})|\Psi_{\text{bound}}^{3N}\rangle + tG_0P|U\rangle. \quad (4.3)$$

The corresponding nuclear matrix elements are then given by

$$\begin{aligned} N_{Nd}^\mu &= \langle \Phi_d | (1+P)J^\mu(\vec{Q}) | \Psi_{\text{bound}}^{3N} \rangle + \langle \Phi_d | P | U \rangle, \\ N_{Npn}^\mu &= \langle \Phi_0 | (1+P)J^\mu(\vec{Q}) | \Psi_{\text{bound}}^{3N} \rangle + \langle \Phi_0 | (1+P) | U \rangle, \end{aligned} \quad (4.4)$$

with NN t -matrix in the 3N space, G_0 the free 3N propagator and P the permutation operator $P = P_{12}P_{23} + P_{13}P_{23}$. Further, $|\Phi_d\rangle$ is the antisymmetrized product state containing the deuteron and the momentum state for the relative motion of the third nucleon. Finally, $|\Phi_0\rangle$ is the antisymmetrized product state describing the two relative motions among the three outgoing nucleons. For details about the solution of Eqs (4.3)–(4.4), see Ref. [11]. It is important to mention that these equations are solved in the partial wave basis. In the following, we, therefore, briefly discuss the partial wave decomposition of the current operator which can generally be written in the form

$$J^\mu = J^\mu(1) + J^\mu(2) + J^\mu(3) + J^\mu(2,3) + J^\mu(3,1) + J^\mu(1,2). \quad (4.5)$$

There are three pairs in the 3N system, but it is sufficient to include a contribution just from one pair exploiting the fully antisymmetric nature of the 3N states. The two-nucleon current operator $J^\mu(2,3)$ is defined according to Eq. (2.5). Compared to Eq. (2.8), in the case of the 3N system, we have additional contributions from the T_1 isospin structure. Thus, the non-vanishing contributions emerge from

$$\vec{J}_{2\pi}(2,3) = \sum_{\beta=3}^{10} f_1^\beta(\vec{q}_2, \vec{q}_3) T_1 \vec{O}_\beta + \sum_{\beta=3}^{10} f_2^\beta(\vec{q}_2, \vec{q}_3) T_2 \vec{O}_\beta + f_3^2(\vec{q}_2, \vec{q}_3) T_3 \vec{O}_2, \quad (4.6)$$

where \vec{q}_2 and \vec{q}_3 are the momentum transfers of nucleons 2 and 3, respectively. We utilize the so-called jI coupling scheme for the 3N basis states

$$|pq\alpha\rangle = \left| pq(ls)j\left(\lambda\frac{1}{2}\right)I(jI)JM \right\rangle \left| \left(t\frac{1}{2}\right)TM_T \right\rangle \equiv |pq\alpha_J\rangle | \alpha_T \rangle. \quad (4.7)$$

Here, l , s , j and t refer to the orbital angular momentum, spin, total angular momentum and isospin of the (2-3) subsystem, respectively. The angular momentum of nucleon 1 is coupled with its spin $\frac{1}{2}$ to the total angular momentum I . Finally, the subsystem total angular momentum j is coupled with I to give the total 3N angular momentum J with the projection M . Similar coupling in the isospin space leads to the total 3N isospin T with the corresponding magnetic quantum number M_T .

Analogously to the procedure described in section II, we compute the general matrix element of the 2N current in the 3N basis

$$\begin{aligned}
\langle p'q'\alpha' | \vec{J}_{2\pi}(2,3) | pq\alpha \rangle &= \langle p'q'\alpha_{J'} | \vec{O}_\beta f_\eta^\beta(\vec{q}_2, \vec{q}_3) | pq\alpha_J \rangle \langle \alpha_{T'} | T_\eta | \alpha_T \rangle \\
&= \sum_{m_j, m_{j'}} C(j'I'J'; m_{j'}, M' - m_{j'}, M') C(jIJ; m_j, M - m_j, M) \\
&\times I_{23}(p', p, Q; (l's')j'm_{j'}, (ls)jm_j) \\
&\times I_1\left(q', q, Q; \left(\lambda'\frac{1}{2}\right) I'M' - m_{j'}, \left(\lambda\frac{1}{2}\right) IM - m_j\right) \langle \alpha_{T'} | T_\eta | \alpha_T \rangle
\end{aligned} \tag{4.8}$$

with

$$\begin{aligned}
I_{23}(p', p, Q; (l's')j'm_{j'}, (ls)jm_j) &= \int d\hat{p}' \int d\hat{p} \sum_{m_{l'}} \sum_{m_l} C(l's'j'; m_{l'}, m_{j'} - m_{l'}, m_{j'}) Y_{l', m_{l'}}^*(\hat{p}') \\
&\times C(ls j; m_l, m_j - m_l, m_j) Y_{l, m_l}(\hat{p}) f_\eta^\beta(\vec{q}_2, \vec{q}_3) \langle s' m_{j'} - m_{l'} | \vec{O}_\beta | s m_j - m_l \rangle
\end{aligned} \tag{4.9}$$

and

$$I_1\left(q', q, Q; \left(\lambda'\frac{1}{2}\right) I'M' - m_{j'}, \left(\lambda\frac{1}{2}\right) IM - m_j\right) = \int d\hat{q}' \mathcal{Y}_{\lambda'\frac{1}{2}}^{I', M' - m_{j'}}(\hat{q}') \frac{\delta(q - |\vec{q}' + \frac{1}{3}\vec{Q}|)}{q^2} \mathcal{Y}_{\lambda\frac{1}{2}}^{I, M - m_j}\left(\widehat{\vec{q}' + \frac{1}{3}\vec{Q}}\right), \tag{4.10}$$

where we have introduced

$$\mathcal{Y}_{\lambda\frac{1}{2}}^{I\nu}(\hat{q}) \equiv \sum_m C\left(\lambda\frac{1}{2}I; m, \nu - m, \nu\right) Y_{\lambda, m}(\hat{q}) \left|\frac{1}{2}\nu - m\right\rangle. \tag{4.11}$$

For I_{23} , we recognize the same type of a matrix element we dealt with in the 2N space. Now, however, the isospin part is separated out. This is because there are much more isospin combinations in the 3N system compared to processes on the deuteron which has the total isospin zero. This separation allows us, in particular, to calculate I_{23} once and use it both for the reaction on ${}^3\text{He}$ and ${}^3\text{H}$. For the numerical implementation it is, however, still important to use the properties of the matrix elements $\langle \alpha_{T'} | T_\eta | \alpha_T \rangle$ ($\eta = 1, 2, 3$) in order to reduce the number of necessary four-fold integrals in I_{23} , even if the isospin dependence is now treated separately. Below we give the matrix elements of the three isospin operators in the 3N isospin space. As already mentioned, we assume that the operators act on the 3N bound state (${}^3\text{He}$ or ${}^3\text{H}$), which has the total isospin $T = 1/2$. It is then straightforward to obtain

$$\begin{aligned}
\left\langle \left(t'\frac{1}{2}\right) T' m_{T'} \left| T_1 \right| \left(t\frac{1}{2}\right) \frac{1}{2} m_T \right\rangle &\equiv \left\langle \left(t'\frac{1}{2}\right) T' m_{T'} \left| (\vec{\tau}(2) + \vec{\tau}(3))_3 \right| \left(t\frac{1}{2}\right) \frac{1}{2} m_T \right\rangle \\
&= C\left(1, \frac{1}{2}, T'; 0, m_T, m_{T'}\right) \sqrt{12} \sqrt{(2t'+1)(2t+1)} \left\{ \begin{matrix} 1 & t & t' \\ \frac{1}{2} & T' & \frac{1}{2} \end{matrix} \right\} \left\{ \begin{matrix} 1 & \frac{1}{2} & \frac{1}{2} \\ \frac{1}{2} & t' & t \end{matrix} \right\} \\
&\times (-1)^{t+t'+\frac{1}{2}+T'} \left(1 + (-1)^{t+t'}\right),
\end{aligned} \tag{4.12}$$

$$\begin{aligned}
\left\langle \left(t'\frac{1}{2}\right) T' m_{T'} \left| T_2 \right| \left(t\frac{1}{2}\right) \frac{1}{2} m_T \right\rangle &\equiv \left\langle \left(t'\frac{1}{2}\right) T' m_{T'} \left| (\vec{\tau}(2) - \vec{\tau}(3))_3 \right| \left(t\frac{1}{2}\right) \frac{1}{2} m_T \right\rangle \\
&= C\left(1, \frac{1}{2}, T'; 0, m_T, m_{T'}\right) \sqrt{12} \sqrt{(2t'+1)(2t+1)} \left\{ \begin{matrix} 1 & t & t' \\ \frac{1}{2} & T' & \frac{1}{2} \end{matrix} \right\} \left\{ \begin{matrix} 1 & \frac{1}{2} & \frac{1}{2} \\ \frac{1}{2} & t' & t \end{matrix} \right\} \\
&\times (-1)^{t+t'+\frac{1}{2}+T'} \left(1 - (-1)^{t+t'}\right),
\end{aligned} \tag{4.13}$$

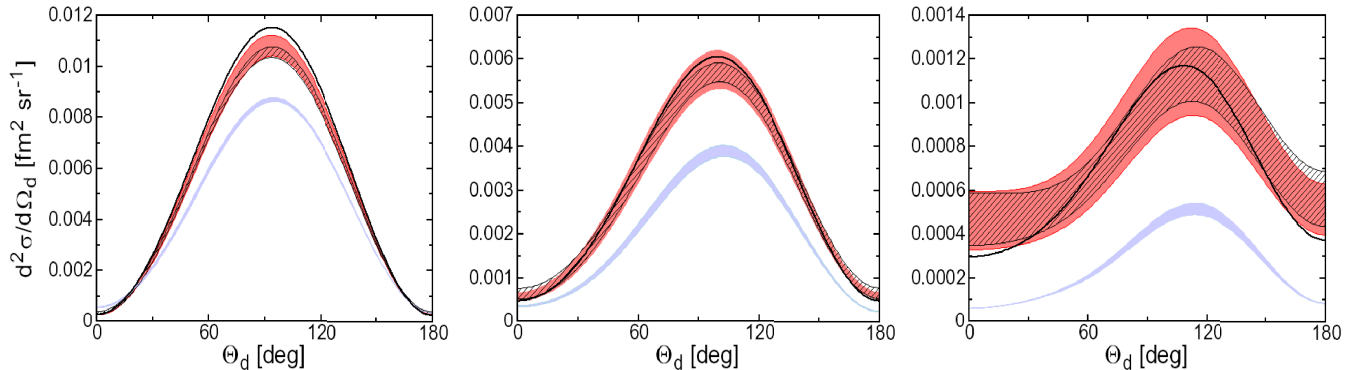


FIG. 4: (color online) Differential cross section in the laboratory frame for ${}^3\text{He}$ two-body photodisintegration at the photon laboratory energies $E_\gamma = 12$ MeV (left), $E_\gamma = 20.5$ MeV (middle) and $E_\gamma = 50$ MeV (right). The band covers N²LO chiral predictions for different cut-off parameter values. The light (blue) band covers results obtained with the single-nucleon current. In the case of the hatched band, the current operator is taken as a sum of the single nucleons current and one-pion exchange current. The dark (pink) band covers N²LO chiral predictions for different cut-off parameter values and the current operator is taken as a sum of the single nucleons current, one-pion exchange current and two-pion exchange current. The solid line represents predictions obtained with the AV18 nucleon-nucleon potential and the related exchange currents [11].

$$\begin{aligned}
 \left\langle \left(t' \frac{1}{2} \right) T' m_{T'} \left| i T_3 \left(t \frac{1}{2} \right) \frac{1}{2} m_T \right\rangle &\equiv \left\langle \left(t' \frac{1}{2} \right) T' m_{T'} \left| i (\vec{\tau}(2) \times \vec{\tau}(3))_3 \left(t \frac{1}{2} \right) \frac{1}{2} m_T \right\rangle \right. \\
 &= C \left(1, \frac{1}{2}, T'; 0, m_T, m_{T'} \right) 12\sqrt{3} \sqrt{(2t'+1)(2t+1)} \begin{Bmatrix} 1 & t & t' \\ \frac{1}{2} & T' & \frac{1}{2} \end{Bmatrix} \begin{Bmatrix} 1 & 1 & 1 \\ \frac{1}{2} & \frac{1}{2} & t \\ \frac{1}{2} & \frac{1}{2} & t' \end{Bmatrix} \\
 &\times (-1)^{1+t+\frac{1}{2}+T'}. \tag{4.14}
 \end{aligned}$$

V. RESULTS FOR PHOTODISINTEGRATION OF ${}^3\text{He}$

We are now in the position to discuss our results for two- and three-body photodisintegration of ${}^3\text{He}$ at three example photon laboratory energies $E_\gamma = 12, 20.5$ and 50 MeV. The Coulomb force between two-protons in three-nucleon scattering states is not taken into account. The three-nucleon matrix elements \vec{N} are obtained using the partial wave decomposition, with the total angular momentum of the three-nucleon system $J \leq 15/2$ and including all partial waves with the subsystem total angular momentum $j \leq 3$. The nuclear matrix elements \vec{N} are computed as using the formalism described in section IV. Given \vec{N} , one can calculate cross sections and polarization observables which are expressed in terms of the nuclear matrix elements with different spin projections carried by the initial photon, the ${}^3\text{He}$ nucleus and the outgoing nucleons and/or deuteron. For more details we refer the reader to Refs. [5, 11]. In the following we just present our sample results for the chiral EFT approach.

We begin with the exclusive unpolarized cross section for two-body breakup of ${}^3\text{He}$, $d^2\sigma/d\Omega_d$, where the final deuteron would be observed. It is depicted in Fig. 4 as a function of the deuteron scattering angle θ_d defined with respect to the initial photon direction at the photon laboratory energies $E_\gamma = 12, 20.5$ and 50 MeV. We observe a similar behaviour as compared to the differential cross section in photodisintegration of the deuteron. The single nucleon current contribution yields significantly lower values as compared to the ones which include MECs. The TPE bands overlap with the OPE bands and appear to be broader than the OPE bands. As expected, the bands become wider with increasing photon energy.

Next, the results for a few polarization observables are shown in Fig. 5. We consider the photon ($A_x^\gamma(\theta_d)$) and the ${}^3\text{He}$ ($A_y^{3\text{He}}(\theta_d)$) analyzing powers as well as the spin correlation coefficients $C_{x,y}^{\gamma,3\text{He}}(\theta_d)$ and $C_{y,x}^{\gamma,3\text{He}}(\theta_d)$. In the case of the photon analyzing power $A_x(\gamma)$, the prediction bands for the single nucleon current give higher values than the other, more complete calculations, but the shape of the bands are always similar. The TPE bands are broader than OPE bands and overlap with them. For the ${}^3\text{He}$ analyzing power $A_y({}^3\text{He})$ and the spin correlation coefficients C_{XY} and C_{YX} , we observe that the results based on chiral EFT generate very broad prediction bands, especially at the highest energy considered. Interestingly, the results based on the single-nucleon current for these observables are completely different from the ones involving the MEC. This suggests that these observables are very sensitive to the details of the meson exchange currents, and their proper description will require the inclusion of the subleading OPE

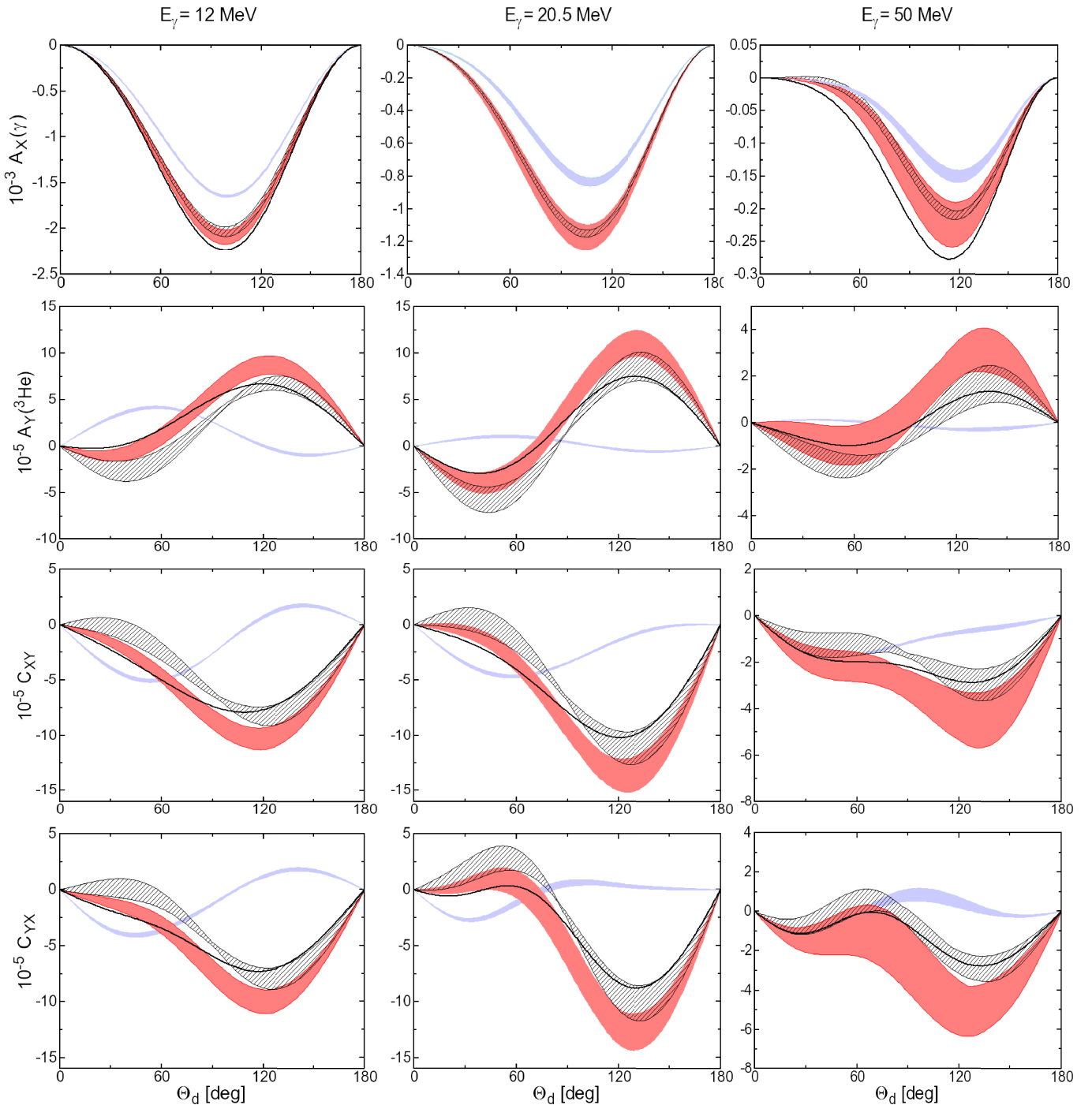


FIG. 5: (color online) Spin observables for ${}^3\text{He}$ two-body photodisintegration at photon laboratory energy $E_\gamma = 12$ MeV (left), $E_\gamma = 20.5$ MeV (middle) and $E_\gamma = 50$ MeV (right). The upper rows show the analyzing powers for photon ($A_X(\gamma)$) and ${}^3\text{He}$ ($A_Y({}^3\text{He})$). The lower rows show spin correlation coefficients: C_{XY} and C_{YX} . The bands and lines have the same meaning as in Fig. 4.

and short-range contributions not considered in the present work. We further emphasize that the results based on the AV18 potential and the corresponding MEC agree with the (present) chiral EFT calculation.

For the three-body breakup of ${}^3\text{He}$, we only show the semiexclusive differential cross section $d^3\sigma/d\Omega_p dE_p$ (where only one proton would be detected at 15 degrees with respect to the photon beam) at three photon laboratory energies $E_\gamma = 12, 20.5$ and 50 MeV. The calculated cross section is shown as a function of the proton energies in Fig. 6. For the lower photon energy (left panel), the obtained bands appear to be relatively narrow, especially for higher proton

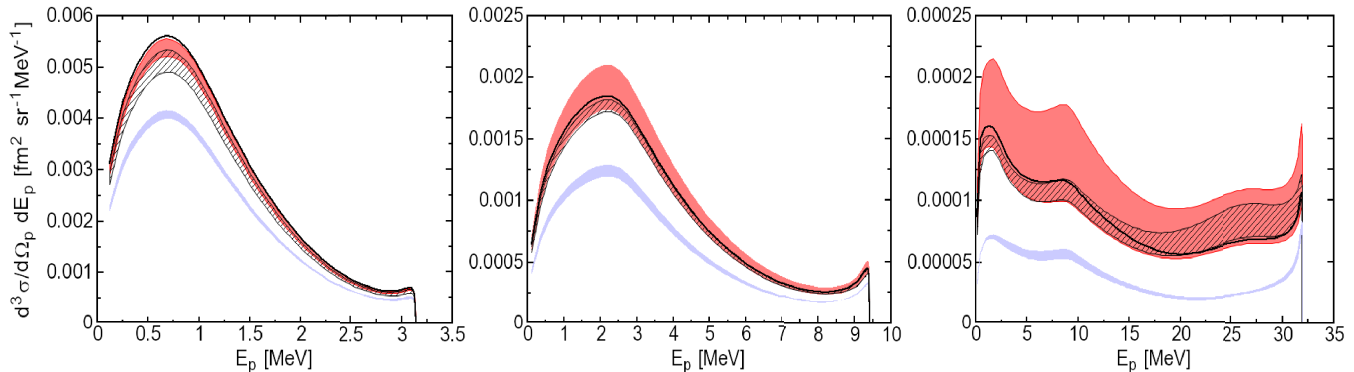


FIG. 6: Differential cross section for semiexclusive ${}^3\text{He}$ three-body photodisintegration ${}^3\text{He}(\gamma, p)pn$ for proton emissions at $\theta = 15^\circ$ and photon laboratory energy $E_\gamma = 12$ MeV (left), $E_\gamma = 20.5$ MeV (middle) and $E_\gamma = 50$ MeV (right). The bands and lines have the same meaning as in Fig. 4.

energies, where they both coincide with the AV18 results. For the lower proton energy the bands become broader. The TPE contributions bring the results close to the one obtained within the conventional framework. The situation is quite different for the highest photon energy (right panel). The shape of the calculated cross section is much more complicated in this case. Further, the band resulting from the TPE parts of the current operator appears to be very broad in the whole range of the proton energies. It remains to be seen whether the inclusion of the missing meson exchange current contributions will allow to reduce the theoretical uncertainty for the cross section.

VI. CONCLUSIONS

In this work we explored the effects of the TPE currents derived recently in the framework of ChEFT [16] in the deuteron and ${}^3\text{He}$ photodisintegration reactions. We studied the role of various ingredients of the chiral 2N current operator in the unpolarized cross section and several polarization observables. As a main outcome of our study, we found that the new terms in the exchange current operator beyond the well-known one-pion exchange contribution play an important role for nearly all considered reactions. In particular, the differential cross section and the photon analyzing power in the deuteron photodisintegration process and the spin observables in ${}^3\text{He}$ two-body photodisintegration are found to provide excellent testing ground for probing the fine details of the exchange current operator.

We also found that the inclusion of the TPE contribution to the current operator alone typically results in very broad bands for the considered observables. This behavior is not unexpected. The OPE and TPE MEC are computed in the framework of chiral EFT within the low-momentum expansion and thus feature singular behavior at short distances (or large momenta). This leads to the observed large sensitivity of the calculated nuclear matrix elements to the short-distance behavior of the corresponding wave functions which is strongly scheme and cut-off dependent. In a *complete* calculation, the cut-off dependence of the low-energy observables is expected to be strongly reduced by the "running" of the corresponding short-range current operators, see e.g. Ref. [27] for the explicit examples of such a behavior in the case of the M1 properties of light nuclei within the hybrid approach and Ref. [28] for an extensive discussion on the (meaning of) renormalization in the context of nuclear EFT with a finite cut-off. Thus, the strong cut-off dependence in the obtained incomplete results which do not include the short-range contributions to the current operator should not be surprising. We expect that a complete NLO calculation including the short-range contact and the subleading OPE contributions to the 2N current operator will yield much narrower bands allowing for a quantitative description of electromagnetic reactions in a wider kinematical range. Work along these lines is in progress.

Acknowledgments

This work was supported in part by the Polish Ministry of Science and Higher Education (grants N N202 104536, N N202 077435), the Helmholtz Association (contract number VH-NG-222) and the European Research Council (ERC-2010-StG 259218 NuclearEFT). The numerical calculations have been performed on the supercomputer cluster of the JSC, Jülich, Germany.

-
- [1] T. S. Park, D.-P. Min, and M. Rho, Phys. Rept. **233**, 341 (1993).
- [2] T. S. Park, K. Kubodera, D. P. Min and M. Rho, Phys. Lett. **B472**, 232 (2000).
- [3] M. Walzl and U.-G. Meißner, Phys. Lett. **B513**, 37 (2001).
- [4] D. Phillips, PoS CD09, 066 (2009).
- [5] R. Skibiński, J. Golak, H. Witała, W. Glöckle, A. Nogga, E. Epelbaum, Acta Phys. Polon. **B37**, 2905 (2006).
- [6] D. Shukla, A. Nogga and D. R. Phillips, Nucl. Phys. **A819**, 98 (2009).
- [7] H. Arenhövel and M. Sanzone, Few-Body Sys. Suppl. **3**, 1 (1991).
- [8] R. Gilman and F. Gross, J. Phys. G, Nucl. Part. Phys. **28**, R37 (2002).
- [9] J. Carlson, R. Schiavilla, Rev. Mod. Phys. **70**, 743 (1998).
- [10] L. E. Marcucci, L. E. Marcucci, A. Kievsky, L. Girlanda, S. Rosati, M. Viviani, Phys. Rev. C **80**, 034003 (2009).
- [11] J. Golak, R. Skibiński, H. Witała *et al.*, Phys. Rept. **415**, 89 (2005) and references therein.
- [12] E. Epelbaum, Prog. Part. Nucl. Phys. **57**, 654 (2006).
- [13] E. Epelbaum, H.-W. Hammer, U.-G. Meißner, Rev. Mod. Phys. **81**, 1773 (2009).
- [14] S. Pastore, R. Schiavilla, and J.L. Goity, Phys. Rev. C **78**, 064002 (2008).
- [15] S. Pastore, L. Girlanda, R. Schiavilla, M. Viviani, R. B. Wiringa, Phys. Rev. C **80**, 034004 (2009).
- [16] S. Kölling, E. Epelbaum, H. Krebs, U.-G. Meißner, Phys. Rev. C **80**, 045502 (2009).
- [17] V. V. Kotlyar, Few Body Syst. **28**, 35 (2000).
- [18] L. L. Foldy and J. A. Lock, in *Mesons In Nuclei*, edited by M.Rho and D. Wilkinson (North-Holland, Amsterdam, 1979), Vol. II.
- [19] W. Glöckle, *The Quantum Mechanical Few-Body Problem* (Springer-Verlag, Berlin/Heidelberg, 1983).
- [20] J. Golak, D. Rospędzik, R. Skibiński *et al.*, Eur. Phys. J. A **43**, 241 (2010).
- [21] R. B. Wiringa, V. G. J. Stoks, R. Schiavilla, Phys. Rev. C **51**, 38 (1995).
- [22] D. O. Riska, Phys. Scr. **31**, 107 (1985).
- [23] D. O. Riska, Phys. Scr. **31**, 471 (1985).
- [24] I. A. Rachek *et al.*, Phys. Rev. Lett. **98**, 182303 (2007).
- [25] S. Ying, E. M. Henley and G. A. Miller, Phys. Rev. C **38**, 1584 (1988).
- [26] A. Nogga, A. Kievsky, H. Kamada, W. Glöckle, L. E. Marcucci, S. Rosati, M. Viviani, Phys. Rev. C **67** 034004 (2003).
- [27] Y. -H. Song, R. Lazauskas, T. -S. Park, D. -P. Min, Phys. Lett. **B656**, 174 (2007).
- [28] G. P. Lepage, arXiv:nucl-th/9706029.